Precursor Photoexcitation and Photoionization of Argon in Shock Tubes

RICHARD A. DOBBINS*
Division of Engineering and Center for Fluid Dynamics, Brown University, Providence, R. I.

A chemical kinetic model describing photochemical reactions that are likely to be important in "cold" argon ahead of a strong shock wave in a shock tube is examined on a quantitative basis. The model includes the propagation of resonance radiation far from the shock front in the wings of the resonance absorption line, imprisonment of the absorbed resonance radiation, subsequent photoionization of excited atoms, photoionization of ground state argon, and certain recombination and de-excitation processes. Specific consideration is given to shock tube geometry, the finite extent of the equilibrium region and the (experimentally) known shock tube wall reflectivity. Theoretical predictions of excited atom and argon ion concentrations in the precursor region are presented for typical shock tube operating conditions. The regimes favorable to the production of argon ions by photoionization of ground state argon and by photoionization of photoexcited argon, respectively, are delineated.

Nomenclature

A_{21} = spontaneous emission probability
$B_\nu(T^{(i)})$ or $B(\nu_{i2},T^{(i)})$ = Planck function evaluated at temperature $T^{(i)}$
c = speed of light
c_{r1},c_{r2} = first and second reflectivity constants
e = charge on an electron
f = oscillator strength
g_1 = statistical weight of ground state
g_2 = statistical weight of excited state
$g_{f2}(\nu)$ = Gaunt factor for photoionization cross section of excited state
g_{t2} = escape probability from radiation imprisonment theory
h = Planck's constant
$\mathcal{I}$ = impurity concentration in parts per million
I_ν = specific spectral intensity
J_ν = average spectral intensity
K_0 = absorption coefficient at center frequency of a spectral line
k = Boltzmann constant
$K_\nu^{(i)}$ = spectral absorption coefficient
L = distance between shock wave pressure discontinuity and contact surface
L_1 = distance between the pressure discontinuity and the equilibrium front
L_2 = distance between equilibrium front and the contact surface
M = Mach number of shock wave
m_e = mass of an electron
n_{a1} = number of ground state atoms per unit volume
n_{a2} = number of excited state atoms per unit volume
n_{a+} = number of argon ions per unit volume
n^* = effective principal quantum number
Q_{12} = photoexcitation rate from state 1 to state 2
Q_{2i} = photoionization rate from state 2 to state i
$p^{(1)}$ = pressure upstream of shock wave
R = shock tube radius
R_y = Rydberg constant
$S^{(i)}$ = line strength
$T^{(i)}$ = temperature in region i
T_{A0} = frozen flow temperature behind the shock wave
$u^{(1)}$ = velocity of gas approaching shock wave as measured in coordinates fixed in the wave
x = distance from shock front
x' = distance from the equilibrium region
$\alpha^{(2)}$ = degree of ionization in the equilibrium region
α_L = semi-half width due to Lorentz broadening
Δ = frequency interval
ζ = distance measured in ratio x'/R
η = distance measured in ratio x/R
θ = arctangent of R/x'
κ_λ = atomic absorption coefficient
λ = wavelength
λ_{21} = wavelength corresponding to frequency ν_{21}
ν = frequency
ν_{21} = frequency of radiation accompanying de-excitation from excited state to ground state
ν_{i2} = frequency of radiation accompanying recombination to first excited state
ν_{i1} = frequency of radiation accompanying recombination to ground state
$\xi(\nu,T^{(2)})$ = Gaunt factor for emission defined in text
$\sigma_1(\nu)$ = photoionization cross section of ground state argon
$\sigma_2(\nu)$ = photoionization cross section of excited argon
$\tau\nu$ = optical depth
ϕ_+ = dimensionless ion concentration
ϕ_2 = dimensionless excited state concentration
ψ = L_2/R
$\rho^{(i)}$ = gas density
ω = solid angle

Specie subscripts

1 = ground state
2 = excited state

Superscripts

1 = conditions upstream of the shock front
2 = equilibrium conditions downstream of the shock front
i = conditions at 1 or 2

Presented as Paper 68-666 at the AIAA Fluid and Plasma Dynamics Conference, Los Angeles, Calif., June 24–26, 1968; submitted January 20, 1969; revision received August 11, 1969. This study was performed while the author was on sabbatical leave at the California Institute of Technology. The author is deeply indebted to D. Schlüter, Sternwarte Bergedorf, Hamburg, for the information on photoionization cross sections generously conveyed prior to publication. The advice and encouragement of the staff of the Guggenheim Jet Propulsion Center, California Institute of Technology, with whom the author was privileged to spend his sabbatical leave, is also acknowledged. This research was supported by the Air Force Office of Scientific Research (OAR) under Contract AF 49(638)-1285 and, in part, by Project Squid, Contract 4965-20.

* Professor. Member AIAA.

I. Introduction

THE discovery of precursor electrons ahead of strong shock waves in argon contained in shock tubes in which the driver is a compressed light gas is well documented.† Two of the earlier reports on electron precursors that appeared almost simultaneously were by Weymann[1] and by Gloerson,[2] and the former credits R. M. Hollyer as being the first to report precursor effects in a document dated May 1957. There has been experimental progress toward defining the level of the precursor electron concentration on a quantitative basis. Probably one of the more carefully conducted experimental studies of the electron concentration ahead of a shock wave in argon in a gas-driven shock tube is that of Lederman and Wilson,[3] whose measurements were made with a tuned microwave cavity.

In the period intervening between the dates of the work of Weymann and Lederman-Wilson there have been many theoretical studies attempting to explain these observations. Physical mechanisms first proposed were photoelectric effect and diffusion of electrons from behind the shock front.[1,2] Wetzel[4] concluded that gradient type diffusion of electrons could not produce the effects that had been observed. He later suggested that photoionization of ground state argon could be the important mechanism[5] and this effect has been further analyzed by Clarke and Ferrari.[6]

Photoionization of ground state argon proves to be less important at higher densities because the photon mean free path for radiation of the relevant frequency is very small. On the other hand, the resonance line radiation emitted by the hot gas can propagate very large distances in the wings of the resonance absorption line in the cold gas. Once a photon of resonance radiation is absorbed, it will soon be re-emitted with high probability near the center of the line where the photon mean free path is again very small and its escape to the wall of the shock tube is impeded. This latter condition is referred to as the imprisonment of radiation. (The term "imprisonment of radiation" as used by Holstein[7] specifically applies to the propagation of line radiation possessing a photon mean free path at the center of the line very small compared with the dimensions of the container enclosing the gas. The term "radiation trapping" is often used to describe the same effect but the latter term is also used to describe different effects relating to the absorption of radiation.) Thus, the propagation of energy in the wing of the resonance line combined with subsequent imprisonment provide a mechanism that can operate to cause electronic excitation at distances far ahead of the shock wave.

The literature of the Russian investigators in this area has recognized these concepts from the outset. Biberman and Veklenko,[8] as early as 1960, predicted electronic "excitation temperature" one meter ahead of the shock wave only slightly less than the equilibrium temperature behind the shock wave. Lagar'kov and Yakubov[9] proposed in 1962 that photoionization of excited argon would lead to appreciable concentrations of electrons ahead of the shock wave. Tumakaev and Luzovskaya[10] described in 1965 what appears to be the first test of the prediction of electronically excited species ahead of a shock wave in mercury vapor. In a similar vein, Murty[11] of the Indian Institute of Science recently examined the role of line radiation on precursor ionization. His model was a shock wave of infinite extent in a hydrogenic gas, and it included the occurrence of photoexcitation by line radiation.

We wish to study precursor effects in argon within the context of a kinetic model that includes the aforementioned mechanisms. In almost all previous studies of shock wave precursors and structure, the waves have been considered to be infinite in extent. The analysis for the infinite shock wave can be applied directly to shock tube experiment when only viscosity and heat conduction are included. This is obviously not the case when radiative effects become important. Our model should take advantage of the relative abundance of information available on argon that has originated from studies in gaseous discharges, electron beams, and arc jets. While we recognize that the precursor is itself a portion of the shock structure, we will treat it as an appendage that may be isolated for separate analysis. Finally, our aim is to learn of the production excited states and electron-ionic argon pairs, or simply argon ions, rather than the production of electrons as has been emphasized in the experimental works just cited. Our results will be more pertinent to future studies that might employ devices to measure ions (mass spectrometers) and excited states (optical spectrometers) than it is to past studies with devices that measured electron density. We adopt this viewpoint because electrons can be produced by many processes, some of which are mentioned below, whereas precursor excited states and ions are usually only produced by those mechanisms that operate in the structure of a shock wave that is influenced by radiative effects.

† A large body of literature on the occurrence of precursors in electrically-driven shock tubes is excluded from consideration.

II. Photochemical Kinetic Model and Kinetic Rates

We consider the shock wave to consist of a precursor region terminated by the translational shock wave or shock front, a collisional relaxation region, and a more extensive region also of finite extent where the state of the gas is given by the application of equilibrium thermodynamics and the jump conditions that express conservation of mass, momentum, and energy. The equilibrium region is terminated by the contact surface (see Fig. 1). Our aim will be to predict the concentration of excited and ionized species on the axis of the circular shock tube in the precursor region at a distance $\zeta = x/R$ ahead of the shock front. In our model we consider argon to exist either in the ground state ($3p^6\ {}^1S_0$), or in an excited state ($3p^5\ 4s\ {}^1P_1$), or as an ion in the ${}^2P^0_{3/2}$ state. These states are represented by the subscripts 1, 2, and i, respectively. Thus, all upper singlet states, all excited triplet and ionic states are ignored. Figure 2 shows schematically the simplified emission spectra vs. frequency of the hot gas.

We will be interested in examining the following series of photochemical reactions that may be expected to occur in the precursor region:

1) Production of excited species (Ar_2) through photoexcitation of ground state atoms (Ar_1) by propagation of the resonance radiation, ν_{21}, from behind the shock front,

$$Ar_1 + h\nu_{21} \xrightarrow{Q_{12}} Ar_2 \tag{1}$$

2) De-excitation of Ar_2 by spontaneous emission in the presence of radiation imprisonment,

$$Ar_2 \xrightarrow{g_{12}A_{21}} Ar_1 + h\nu_{21} \tag{2}$$

3) Photoionization of excited argon by radiation of frequency $\geq \nu_{i2}$,

$$Ar_2 + h\nu \xrightarrow{Q_{2i}} Ar^+ + e^- \tag{3}$$

4) Photoionization of ground state argon by radiation of frequency $\geq \nu_{i1}$,

$$Ar_1 + h\nu \xrightarrow{Q_{1i}} Ar^+ + e^- \tag{4}$$

In addition to this we will comment on two other reactions which appear potentially important:

5) recombination of Ar^+ and e^- by collisional-radiative recombination, and

6) collisional de-excitation of excited argon by electron-excited atom collisions. We discuss in detail the first four of these reactions whose rate constants are indicated earlier.

1. Photoexcitation of Ground State Argon

We evaluate the photoexcitation rate by computing the number of photons absorbed per unit volume in the frequency interval surrounding ν_{21}. This rate is expressed by the integral

$$Q_{12} = 4\pi \int_{\nu_{21}\Delta}^{\nu_{21}+\Delta} \frac{K_\nu^{(1)} J_\nu(\eta)}{h\nu}\, d\nu \tag{5}$$

where the average spectral intensity is given by

$$J_\nu(\eta) = \frac{1}{4\pi} \int I_\nu(\eta,\omega) d\omega \tag{6}$$

We have studied[12] the transfer of resonance radiation propagating along a ray passing through a finite slab of hot gas into a region filled with a cold gas. We find the photoexcitation in the cold gas occurs as a result of absorption in the wings of the (low) pressure-broadened dispersion line. The spectral variation of absorption in the cold gas is therefore given by

$$K_\nu^{(1)} = \alpha_L^{(1)} S^{(1)}/\pi(\nu - \nu_{21})^2 \tag{7}$$

The relationship for the Lorentz semi-half width, α_L, in the cold gas due to low pressure broadening recommended by Breene,[13] and attributed to Fursov and Vlassov,[14] is

$$\alpha_L^{(1)} = \tfrac{2}{3} e^2 f n_{a1}^{(1)}/m_e \nu_{21} \tag{8}$$

We also find that the Doppler shift of the resonance line-center frequency that would result from the relative motion between the hot and cold gases in a shock wave is very small compared to the width of the emission line in the hot gas. The Doppler shift may therefore be neglected in computing the photoexcitation rate in the precursor region. Finally we find that, based on certain assumptions[12] for the mechanisms of line broadening in the hot gas and on estimates of slab thicknesses, the intensity at the interface of the hot and cold gases is the blackbody intensity over the frequency span where absorption occurs in the cold gas. For present purposes we will treat the equilibrium zone as a blackbody emitter in the spectral range near the resonance line although this particular assumption must be improved when circumstances warrant.

The local specific spectral intensity is then given by

$$I_\nu(\theta,x') = B_\nu(T^{(2)}) \exp(-K_\nu x' \sec\theta) \tag{9}$$

In expressing the radiation intensity in the form given by Eq. (9), we have temporarily neglected re-emission in the cold gas which will be considered when the effective de-excitation rate is calculated. We insert Eq. (9) into Eq. (6) to evaluate the average spectral intensity for a circular surface emitter. The result is

$$J_\nu(\eta) = [B_\nu(T^{(2)})/2]\,\{E_2[K_\nu^{(1)} R\eta] - (1+\eta^{-2})^{-1/2} E_2[K_\nu^{(1)}(1+\eta^{-2})^{+1/2} R\eta]\} \tag{10}$$

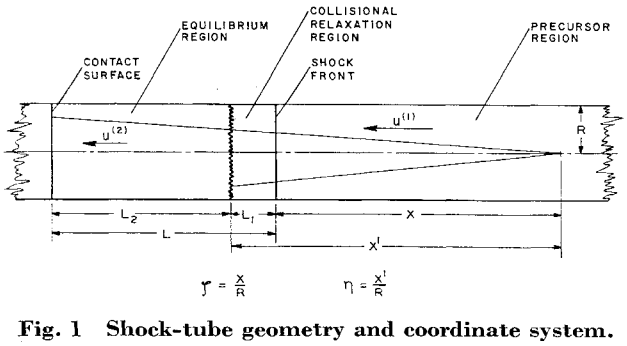

Fig. 1 Shock-tube geometry and coordinate system.

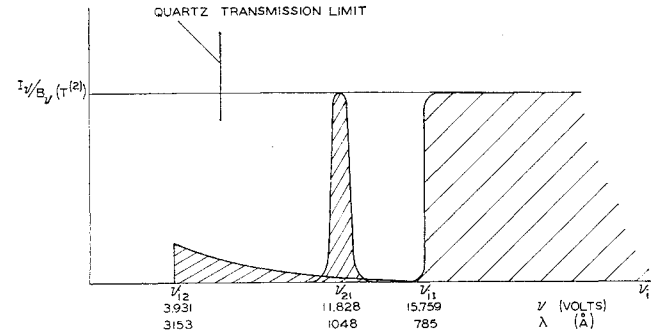

Fig. 2 Schematic diagram of hot gas emission spectrum.

where

$$E_n(\tau_\nu) = \int_1^\infty \frac{\exp(-\tau_\nu z)}{z^n}\, dz$$

The photoexcitation rate can be calculated by inserting Eqs. (7) and (10) into (5). The details of this calculation are given elsewhere[12]; the result is

$$Q_{12} = (4\pi/3) B(\nu_{21}, T^{(2)}) [\alpha_L^{(1)} S^{(1)}/R]^{1/2} f(\eta) \tag{11}$$

where

$$f(\eta) = \eta^{-1/2}[1 - (1+\eta^{-2})^{-3/4}] \tag{12}$$

We note that for $\eta^2 \gg 1$ the shock front emits as a point source and we have

$$f(\eta^2 \gg 1) = \tfrac{3}{4}\, \eta^{-2.5}$$

Thus, we see that a large η^2, the excited specie generation rate decreases as $\eta^{-0.5}$ due to absorption and as η^{-2} due to geometric attenuation. A correction to the geometric factor will be made later to account for the partially reflective property of shock tube walls to radiation that impinges at small angles of incidence.

2. De-Excitation by Spontaneous Emission with Radiation Imprisonment

An excited atom will exist prior to decay to the ground state for an average period of time that is simply the reciprocal of the spontaneous emission rate A_{21}, given by the Einstein theory[15] of radiation. This spontaneous emission rate is

$$A_{21} = (8\pi^2 e^2 g_1 f)/(m_e c \lambda_{21}^2 g_2) \tag{13}$$

At pressures of 10^{-3} atm, the photon emitted by the de-excitation process will be absorbed with high probability in a distance very small compared with the radius of a shock tube. Thus, many successive absorption and re-emission processes are required before the energy created in the original de-excitation process reaches the wall. The process is referred to as radiation imprisonment and it has been extensively studied by Holstein,[7,16,17] Phelps,[18,19] and their colleagues as well as by Biberman[20,21] and his co-workers in Russia. McWhirter[22] has reviewed more recent theoretical results on radiation imprisonment.

Holstein[16] has calculated the probability of escape of imprisoned radiation when the dominant line-broadening mechanism is the (low) pressure broadening in the dispersion portion of the line profile. Using the Fursov-Vlassov relation, Eq. (8), for the Lorentz semi-half width, Holstein's result is expressed[19] as

$$g_{t2} = 1.115/(3^{1/3}\pi)\, [\lambda_{21}/R]^{1/2} = 0.205\, [\lambda_{21}/R]^{1/2} \tag{14}$$

The effective de-excitation rate is simply the product of Eqs. (13) and (14). Thus the transmission equation, Eq. (9), is used to give the initial photoexcitation rate due to the ab-

sorption of resonance radiation that originates in the equilibrium region, and Holstein's solution for cylindrical geometry to the full radiative transfer equation is used to obtain the net de-excitation rate in the cold gas of the precursor region. The theory of radiation imprisonment gives predictions that agree well with experiment in the limited number of tests that have been performed.[17,19]

In adopting Holstein's solution to the transfer of resonance radiation in the cold gas we must fulfill the various imposed assumptions, two of which are worthy of further discussion:

1) The boundary condition used by Holstein in his solution to the resonance radiative transfer is that the gas is enclosed by a nonreflecting wall. We comply with this condition by asserting that the wall is a perfect absorber for resonance radiation that is re-emitted by the cold gas. The angle of incidence of the resonance photons passing to the wall by successive emission and absorption will be nearly normal and the absorptivity of an oxide-coated metallic surface would be expected to be high. Excited atom concentration would be increased in proportion to the reciprocal of one minus reflectivity. Thus, an effective reflectivity of 20% would augment excited state concentration only by 25%.

In a subsequent section, we will treat the wall as partially reflecting in order to account for its influence on radiation from the equilibrium region that impinges upon the wall at grazing angles. In that case, we will offer an operational definition of wall reflectivity and will cite experimental measurements of this quantity.

2) The excited atom concentration will possess both radial and axial gradients and the latter will result in diffusion of excited atoms ahead of the shock wave. We have estimated, a posteriori, the volumetric production of excited atoms by absorption of resonance radiation divided by the diffusive accumulation of the same. We find this ratio to be 10^{+4} or greater for the numerical results cited below, and therefore radiative generation entirely dominates over diffusive accumulation. The local escape probability is therefore influenced only by the radial geometry which is considered by Holstein's theory. The magnitudes of the radial and axial gradients are found to be numerically equal at a distance of about one shock tube diameter from the shock front.

3. Photoionization of Excited Argon

The local rate of photoionization of excited argon is found by evaluating the local rate of absorption of photons in frequency range $\nu_{i2} \leq \nu < \infty$. That is,

$$Q_{2i} = 4\pi \int_{\nu_{2i}}^{\infty} \frac{\sigma_2(\nu) J_\nu(T^{(2)})}{h\nu}\, d\nu \tag{15}$$

The photoionization cross section of excited argon is given by Schlüter[23] in the following form:

$$\sigma_2(\nu) = \frac{64\pi^4 m_e e^{10} \lambda^3 g_{f2}(n,{}^*\epsilon)}{3(3^{1/2}) c^4 h^6 n^{*5}} \tag{16}$$

where the Gaunt factor $g_{f2}(n^*,\epsilon)$ depends on the effective principal quantum number, n^*, and also the electron energy, ϵ, given by

$$\epsilon = 1/R_y\lambda - 1/n^{*2} \tag{17}$$

For the ν_{i2} cutoff frequency of the $^1P_1$ state of argon I, Schlüter[24] gives $n^* = 1.8197$ and $g_{f2}(n^*,0) = 0.01195$. With these numbers we find the photoionization cross section to be 1.67×10^{-19} cm^2, which is in general agreement with an estimate of this cross section given by Lagar'kov and Yakubov.[9] The cross section at higher frequencies is then expressed as

$$\sigma_2(\nu > \nu_{i2}) = \sigma_2(\nu_{i2})\, [\nu_{i2}/\nu]^3\, g_{f2}(\nu)/g_{f2}(\nu_{2i}) \tag{18}$$

where

$$\sigma_2(\nu_{i2}) = 1.67 \times 10^{-19} \text{ cm}^2$$

The radiant intensity in the subordinate continuum, i.e., the ν_{i2} spectral range, is formulated by noting that the optical depth in this spectral region is small compared with unity in both the equilibrium region and the precursor region. The local specific spectal intensity in the form obtained by taking $K_\nu^{(2)} L_2 \ll 1$ and $K_\nu^{(1)} x' \ll 1$ is

$$I_\nu(\theta) = K_\nu^{(2)} L_2 \sec\theta B_\nu(T^{(2)}) \tag{19}$$

We determine the average intensity at a point on the axis of a right circular cylinder a distance η cylinder radii from the equilibrium front. The result of the calculation is

$$J_\nu(T^{(2)}) = \tfrac{1}{4} B_\nu(T^{(2)}) K_\nu^{(2)} L_2 g(\eta) \tag{20}$$

where

$$g(\eta) = 2\left\{\frac{1}{\psi}\left[(\theta_2 - \theta_1) - \eta \ln\frac{\sec\theta_2}{\sec\theta_1}\right] + \ln\sec\theta_1\right\} \tag{21}$$

and

$$\sec\theta_1 = [1 + (\eta + \psi)^{-2}]^{+1/2} \sec\theta_2 = (1 + \eta^{-2})^{+1/2}$$

$$\psi = L_2/R, \text{ and } \eta = x'/R$$

When $\psi \ll \eta$ and $\eta^2 \gg 1$, then the terms in the square bracket vanish and we have $g(\eta^2 \gg 1) \to \eta^{-2}$. Thus, at large distances from the shock front, we recover the inverse square law geometric attenuation for the spectral intensity of the subordinate continuum, which is not strongly absorbed in either the hot or cold gas.

The atomic absorption coefficient, κ_λ, is given by the following equation,[23,25] similar to a corresponding relation due to Unsold,

$$\kappa_\lambda = 6A_1 \frac{kT\lambda^3}{ch} \exp\left\{-\frac{h\nu_{i1}}{kT}\right\}\left[\exp\left(+\frac{h\nu}{kT}\right) - 1\right] \xi(\nu,T) \tag{22}$$

where

$$A_1 = 32\pi^2 e^6/3(3)^{1/2} h^3 c^3$$

In Eq. (22) we have approximated the ratio of the statistical weights of the ion and atom as 6.0, and the factor $\xi(\nu,T)$ represents the quantum mechanical correction factor for departure from hydrogenic behavior.

By combining the Planck function with Eq. (22) multiplied by the ground state atom concentration in the equilibrium region, $n_{a1}{}^{(2)}$, we obtain

$$B_\nu(T) K_\nu^{(2)} = 12 A_1 n_{a1}{}^{(2)} kT^{(2)} \exp\left[-\frac{h\nu_{21}}{kT^{(2)}}\right] \xi(\nu,T^{(2)}) \tag{23}$$

We insert Eqs. (18, 20, and 22) into Eq. (15) and obtain

$$Q_{2i} = A_2 L_2 n_{a1}{}^{(2)} f(T^{(2)}) \sigma_2(\nu_{i2}) g(\eta) \tag{24}$$

where

$$f(T^{(2)}) \equiv T^{(2)} \exp(-S_{i1}{}^{(2)}) G_2(T^{(2)}) \tag{25}$$

$$G_2(T^{(2)}) \equiv 3\int_1^{\infty} \left[\frac{\nu_{i2}}{\nu}\right]^4 \frac{g_{f2}(\nu)}{g_{f2}(\nu_{i2})}\, \xi(\nu,T^{(2)}) d\left[\frac{\nu}{\nu_{i2}}\right] \tag{26}$$

$S_{i1}{}^{(2)} \equiv h\nu_{i1}/kT^{(2)}$, and $A_2 = 128\,\pi^3 e^6 k/3(3)^{1/2} c^3 h^4 = 2.494 \times 10^{+4}$ °K^{-1} sec^{-1}. In the hydrogenic approximation $\xi(\nu,T)$, $g_{f2}(\nu)$, and $G_2(T^{(2)})$ are all equal to unity. In our calculations, we use Schlüter's[23] values of the $\xi(\nu,T)$ function which do not involve the concept of a cutoff frequency. Some values of $\xi(\nu,T)$[23] appropriate to the ν_{i2} frequency range are quoted, along with values of $g_{f2}(\nu)$,[24] in Table 1. With these quantities, we find the Gaunt integral can be expressed as

$$G_2(T^{(2)}) = 0.194(T^{(2)}/10^{+4}) - 0.065 \tag{27}$$

In using Schlüter's $\xi(\nu,T)$ factor, we are including the effect of radiation formed not only by recombination to the first excited state, but also to all higher states when an electron possesses sufficient energy to give rise to radiation in the ν_{i2} frequency range. Thus, while our model accounts for only a single excited state in the cold gas, we do include the effect of all excited states in the hot gas when the spectral quality of the emitted radiation is calculated. It is important to include these components of radiation in the ν_{i2} frequency range because of the small value of the absorption (emission) cross section, $\sigma_2(\nu_{i2})$.

Resonance radiation can also cause photoionization of excited argon. No important contribution to photoionization was found by the resonance radiation in the cases we cite below and we omit this calculation from the present discussion.

4. Photoionization of Ground State Argon

The photoionization of ground state argon is calculated by evaluating the rate of absorption of photons of sufficient energy to cause direct ionization of ground state argon. The rate of absorption of photons of frequency $\nu > \nu_{i1}$ per ground state atom is

$$Q_{1i} = 4\pi \int_{\nu_{i1}}^{\infty} \frac{\sigma_1(\nu) J_\nu}{h\nu} \, d\nu \tag{28}$$

It is reasonable to assume the equilibrium region emits as a black body in the spectral region $\nu_{i1} < \nu < \infty$. For the blackbody emission the average intensity on the axis of the shock tube is again given by Eq. (10).

The photoionization cross section, σ_1, of ground state argon has been measured by Samson,[26] and over a frequency range of from $\nu_{i1} < \nu < \nu_j$, its value is close to 34×10^{-18} cm^2 where $\nu_j = 1.67\ \nu_{i1}$. For the frequency region beyond ν_j where Samson reports a cross that decreases as $\nu^{-5.5}$ we find no contribution of importance in the cases cited below when the integral expressed, Eq. (28), is evaluated from ν_j to ∞ by the method steepest descent. Thus, we express the direct photoionization rate as

$$Q_{1i} = 2\pi\sigma_1 e(\eta) F(\nu_{i1}, S_{i1}^{(2)}) \tag{29}$$

with

$$e(\eta) = E_2(\tau_R \eta) - (1 + \eta^{-2})^{-1/2} E_2[\tau_R \eta (1 + \eta^{-2})^{+1/2}] \tag{30}$$

and

$$F(\nu_{i1}, S_{i1}^{(2)}) = \int_{\nu_{i1}}^{\nu_j} \frac{B_\nu(T^{(2)})}{h\nu} \, d\nu \tag{31}$$

where τ_R is the optical depth based on shock tube radius, $\tau_R = \sigma_1 n_{a1}^{(1)} R$. The upper limit of the integral, Eq. (31), makes no contribution and, therefore, the important frequencies for the production of argon ions are near the cut-off of the primary continuum. The evaluated form of the integral, Eq. (31), is

$$F(\nu_{i1}, S_{i1}^{(2)}) = (2/c^2)\nu_{i1}^3 [e^{-S_{i1}^{(2)}/(S_{i1}^{(2)})^2}] \, [S_{i1}^{(2)} + 2] \tag{32}$$

5. Shock-Tube Reflectivity Function

The photoexcitation rates given earlier have been calculated on the basis that no reflections occur at the shock tube walls. Visual observations of a light source placed inside a metal tube of rather low quality surface finish indicate that wall reflections can substantially augment the radiant intensity over its value in the absence of reflections. This crude test suggests that a more quantitative evaluation of the influence of wall reflectivity may be obtained as follows. The intensity of a stable light source inside a shock tube is measured by a stable, linear photometric transducer as the distance between the source and transducer is varied. The test is then repeated with the shock tube removed and care is exercised to prevent reflections from any surface or light from any foreign source from reaching the receiver. We then define the reflectivity function, $r(\eta)$, as the ratio of the intensities measured with shock tube present to intensity measured with shock tube absent. Ideally, the effective frequency content of the light source should conform, in turn, to the various frequencies which cause photochemical effects. This proves to be nearly impossible because the resonance radiation of argon corresponds the frequencies for which light sources, window materials, and transducers are either nonexistent or difficult to use.

We have performed crude measurements of the shock tube reflectivity function using a light source of one centimeter diameter, a receiver with a sensitive area of 2 cm diam, and a monopass filter which passes radiation at 4190 Å. We found the reflectivity function was approximately expressed by

$$r(\eta) = C_{r1}\eta - C_{r2} \qquad \eta \geq 2 \tag{33}$$

For a round, steel shock tube we found $C_{r1} = 1.11$ and $C_{r2} = 1.0$. A square aluminum tube was found to have a lower reflectivity at large η by factor of seven, but reflectivity was again linear in η.

We multiply these photochemical reaction rates by the reflectivity function to obtain the augmented rate applicable when wall reflectivity is considered. In view of the definition of the reflectivity function, the augmented rate is obtained by replacing the geometric factors, viz., $e(\eta)$, $f(\eta)$, and $g(\eta)$, by their respective products with $r(\eta)$.

Table 1 Selected gaunt factors for argon I

ϵ	g_{f2} for $^1P_1$ argon (Ref. 24)
0.00	0.01195
0.01	0.00955
0.04	0.00423
0.09	0.00238

λ(Å)	$\xi(\lambda,T)$ 8000°K	10,000°K	(Ref. 23) 12,000°K
2900	0.40	0.55	0.70
2600	0.20	0.34	0.47
2300	0.10	0.19	0.30
2000	0.033	0.083	0.15

III. Conservation Equations

We calculate the electron concentration by solving the specie conservation equations for the argon excited atoms and argon ions, respectively,

$$-u^{(1)} \, dn_{a2}/dx = +Q_{12} - g_{f2}A_{21}n_{a2} - Q_{2i}n_{a2} \tag{34}$$

and

$$-u^{(1)} \, dn_{a+}/dx = +Q_{2i}n_{a2} + Q_{1i}n_{a1} \tag{35}$$

We nondimensionalize the equation by means of

$$\phi_2 = n_{a2}/n_{a2}^{(2)}, \ \phi_+ = n_{a+}/n_{a+}^{(2)}, \text{ and } \eta = x/R$$

where

$$n_{a2}^{(2)} = n_{a1}^{(2)} \, (g_2/g_1)e^{-S_{21}^{(2)}}, \text{ and } n_{a+}^{(2)} = \alpha^{(2)} n_{a1}^{(2)}$$

We insert the rate constants in Eq. (34) and (35) and explicitly display the η dependence of the various photochemical rates. We obtain

$$d\phi_2/d\eta = b_1\phi_2 - b_2 f(\eta) r(\eta) + b_3 g(\eta) r(\eta) \phi_2 \tag{36}$$

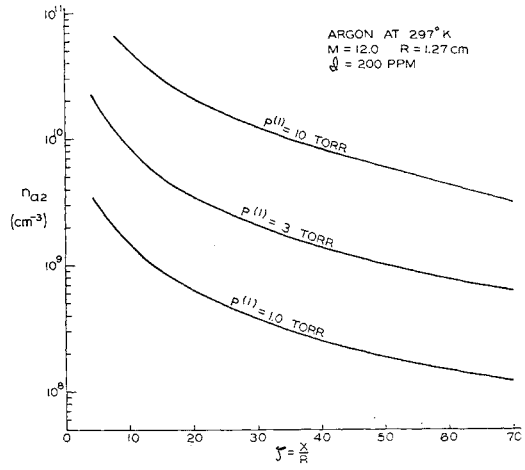

Fig. 3 Excited atom concentration profiles.

with

$$b_1 = 0.205(\lambda_{21}R)^{1/2}(A_{21}/u^{(1)}) \tag{37}$$

$$b_2 = \frac{4\pi}{3}\frac{B(\nu_{21},T^{(2)})}{h\nu_{21}}\left[\frac{\alpha_L{}^{(1)}S^{(1)}}{R}\right]^{1/2}\left[\frac{R}{u^{(1)}n_{a2}{}^{(2)}}\right] \tag{38}$$

$$b_3 = [A_2L_2f(T^{(2)})\sigma_2(\nu_{i2})n_{a1}{}^{(2)}R]/u^{(1)} \tag{39}$$

and

$$d\phi_+/d\eta = -e_1e(\eta)r(\eta) - e_2g(\eta)r(\eta)\phi_2 \tag{40}$$

with

$$e_1 = [2\pi\tau_R F(\nu_{i1},S_{i1}{}^{(2)})]/[u^{(1)}n_e{}^{(2)}] \tag{41}$$

and

$$e_2 = b_3\, n_{a2}{}^{(2)}/n_{a+}{}^{(2)} \tag{42}$$

For the quasi-steady solution, which can be demonstrated to apply soon after the rupture of the diaphragm of the shock tube, the boundary conditions are applied as follows. Equation (36) is solved for ϕ_2 assuming that $d\phi_2/d\eta = 0$ at $\eta = \eta_\infty$ and that the only important terms are those representing photoexcitation $[b_2f(\eta)r(\eta)]$ and spontaneous emission accompanied by radiation imprisonment $(b_1\phi_2)$. Thus, we have ϕ_2 at η_∞ given by

$$\phi_2(\eta) = (b_2/b_1)\, f(\eta)r(\eta) \tag{43}$$

When the full Eq. (36) is solved, we find that ϕ_2 is given with good accuracy by Eq. (43) over a moderate range of η. Thus, the concentration of n_{a2} is primarily controlled by the rates of photoexcitation and de-excitation by spontaneous emission with radiation imprisonment. Furthermore, since the derivative term proves to be small, we may describe the excited state generation as purely photochemical in nature, i.e., a stationary light source of the same frequency content as the shock front would produce the same excited atom distribution.

The boundary condition for Eq. (40) is applied by setting $\phi_+ = 0$ at $\eta = \eta_\infty$. The value of η_∞ should correspond to the distance from the equilibrium region at the time it is first "fully developed" to the point in the precursor region where measurements are performed. This distance is not easy to estimate, but we find the ion concentration is insensitive to the value of η_∞.

IV. Some Numerical Results

In the numerical results that are presented below, the distance between the shock front and the contact surface in the shock tube is given by the following dimensional expression,

$$L = L_1 + L_2 = 4.84\, P^{(1)}R^2[1 - (M - 11)/29] \tag{44}$$

where $P^{(1)}$ is in torr, and R and L in cm. Equation (44) is developed from Mirel's theory[27] for test time in argon-filled shock tubes where, when $P_1R \leq 6$ torr-cm, a laminar wall boundary layer persists.

The length of the collisional relaxation region, L_1, is given by

$$\log_{10}(P^{(1)}L_1/u^{(1)}) = 0.368 \times 10^{+5}/T_{A0} - 0.634 - 0.00846\,\vartheta \tag{45}$$

where $T_{A0}(°K)$ is the frozen flow temperature behind the pressure discontinuity, and the impurity level, ϑ, is in ppm. This equation is fitted to the theoretical predictions of Chubb[28] for pure argon and also fitted to the experimental measurements by Petchek and Byron[29] and Wong and Bershader[30] for impure argon.

In Figs. 3 and 4, we show some excited atom and ion concentration profiles ahead of a shock wave at $M = 12$ in argon in a shock tube of 1 in. diam. Additional parameters relating to the calculations presented in Figs. 3 and 4 are presented in Table 2. Energy levels for argon have been taken from Moore[31] and the oscillator strength, f, of 0.200 given by Knox[32] for the $^1P_1$ state of argon was used. The impurity level, which within the context of the present model influences excited state level only insofar as impurities affect the position of the equilibrium front, has been chosen somewhat high in order to assure the attainment of equilibrium at the lowest pressures. At the highest pressure, we violate the criterion for applicability of laminar boundary layer theory in predicting the length of the test gas L. With this exception, the calculations are for conditions that can be achieved in a double diaphragm or combustion-driven shock tube. For all calculations given below, we used a value of 150 for η_∞ and the reflectivity function given by Eq. (33) with constants as previously cited. Shock jump conditions were taken from DeLeeuw's report.[33]

When Eqs. (36) and (40) are solved, we find that a) the effective radiative de-excitation rate, $g_{i2}A_{21}$, is much higher than de-excitation by electron-excited atom collisions,[11] and b) the photoionization rates are much higher than collisional-radiative recombination rate given by Chen.[34] Thus the production of excited atoms is simply a balance between photoexcitation and spontaneous emission with imprisonment. Photoionization is then simply the integrated effect of one, or occasionally the combination of two, photoionizing reactions.

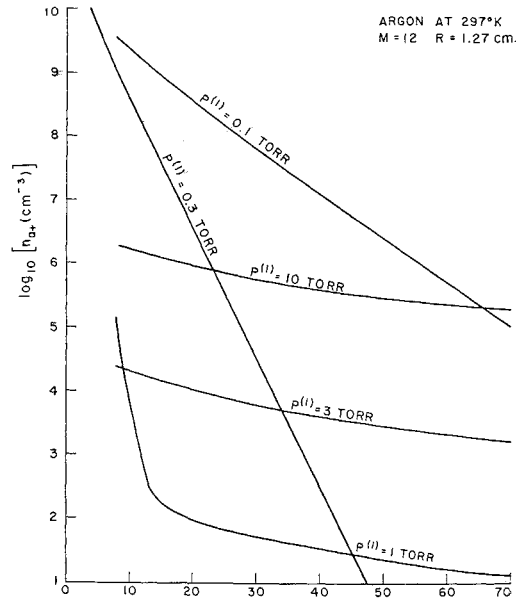

Fig. 4 Argon ion concentration profiles.

Table 2 Additional parameters relating to Figs. 3 and 4 (shock Mach number = 12, $T^{(1)}$ = 297°K, R = 1.27 cm, u_1 = 3.85 × 10^{+5} cm sec^{-1}, C_{r1} = 1.12)

	$P^{(1)}$ torr				
	0.1	0.3	1.0	3.0	10.0
$n_{a1}^{(1)} \times 10^{+16}$ (cm^{-3})	0.325	0.975	3.25	9.75	32.5
g	1000	1000	200	200	200
τ_R	0.140	0.420	1.40	4.21	14.0
L_1, cm	0	0	2.0	0.7	0.2
L_2, cm	0.8	2.3	5.5	21.9	75.2
$T^{(2)}$, °K	9246	9611	10,059	10,484	10,959
$S_{i1}^{(2)}$	19.78	19.03	18.18	17.45	16.69

The results depicted in Figs. 3 and 4 can be best rationalized by seeking solutions to Eqs. (36) and (40) in the limit $\eta^2 \gg 1$ when they can be solved explicitly. We obtain from Eq. (43) for $\eta^2 \gg 1$ when $f(\eta) \to \frac{3}{4}\eta^{-2.5}$ and $r(\eta) \to C_{r1}\eta$, the following expression for the concentration of excited atoms

$$n_{a2} = 0.28 C_{r1} n_{a1}^{(1)} \lambda_{21}^2 (g_2/g_1) \left[B(\nu_{21},T^{(2)})/h\nu_{21}\right] 1/\eta^{1.5} \quad (46)$$

The dimensionless distance η is converted to $\zeta = \eta - L_1/R$ by means of Eq. (45). Figure 3 shows that the n_{a2} concentration increases by a factor of 5 for a three-fold increase in $p^{(1)}$. From Eq. (46) we find that n_{a2} is increased three-fold due to the increase in $n_{a1}^{(1)}$. The remaining factor of 1.7 is contributed by a larger value of the Planck function resulting from an increased $T^{(2)}$.

The argon ion concentration, when the dominant production reaction is the photoionization of photoexcited states, is found by inserting (43) into (40), setting $e_1 = 0$, and integrating. For $\eta^2 \gg 1$ we find $g(\eta) \to 1/\psi\eta - 1/\psi(\eta + \psi)$. The electron concentration is then found as

$$n_{a+} = (0.56\, A_2)(RL_2C_{r1}^2)\left[\frac{\rho^{(2)}(n_{a1}^{(1)})^2}{\rho^{(1)}u^{(1)}}\right] \times \left[\sigma_2(\nu_{i2})\lambda_{21}^2 \frac{g_2}{g_1}\right] f(T^{(2)}) \frac{B(\nu_{21},T^{(2)})}{h\nu_{21}} \frac{1}{\psi^{3/2}} \times \left[\tan^{-1}\left(\frac{\eta}{\psi}\right)^{1/2} + \left(\frac{\psi}{\eta}\right)^{1/2} - \tan^{-1}\left(\frac{\eta_\infty}{\psi}\right)^{1/2} - \left(\frac{\psi}{\eta_\infty}\right)^{1/2}\right] \quad (47)$$

The argon ion concentration for a shock wave with M = 12 is shown in Fig. 4. At the two highest pressures, $p^{(1)}$ = 3 torr and 10 torr, ion concentration is by photoionization of excited atoms and we find argon ion concentration differs by a factor of 100. From Eq. (47) we find this factor of 100 results from a three-fold increase in L_2, a nine-fold increase in $(n_{a1}^{(1)})^2$ and a four-fold increase in the temperature dependent quantity $f(T^{(2)})B(\nu_{21},T^{(2)})$.

At lower pressures the production of argon ions is predominantly by photoionization of ground state atoms. Experimental difficulty in producing equilibrium before the arrival of the contact surface at low pressures is overcome by increasing the impurity concentration. In Fig. 4, we show the argon ion concentration for pressures of 0.1 and 0.3 torr when the impurity concentration has been increased to 1000 ppm. Here we find that the level of ionization produced by photoionization of ground state atoms far exceeds the photoionization of photoexcited atoms at higher pressures. This interesting result suggests that experiments conducted at lower pressures are necessary to reveal the characteristics normally ascribed to photoionization of ground state atoms. These characteristics are principally an exponential decay of argon ion concentration with distance and spatial decay rate of pair concentration that is pressure dependent. Corrections to the emission of the equilibrium region due to a departure from blackbody behavior potentially become important at low pressures.

At low pressures when the photoionization of ground state atoms is dominant, the ion concentration is given by setting $e_2 = 0$ in Eq. (40) and integrating. The result can be expressed as

$$n_{a+} = \frac{2\pi}{u^{(1)}} F(\nu_{i1},S_{i1}^{(2)})\tau_R \int_\eta^{\eta_\infty} e(\eta',\tau_R) r(\eta') d\eta' \quad (48)$$

For $\eta^2 \gg 1$ when $r(\eta) \backsimeq C_{r1}\eta$ and $e(\eta) \to (\frac{1}{2}\eta^2)\exp(-\tau_R\eta)$ Eq. (48) reduces to

$$n_{a+} = \left[\pi\tau_R F(\nu_{i1},S_{i1}^{(2)}) C_{r1}/u^{(1)}\right]\left[E_1(\tau_R\eta) - E_1(\tau_R\eta_\infty)\right] \quad (49)$$

Figure 4 shows an argon ion concentration that increases with decreasing gas density. This effect will continue as gas density decreases until n_{a+} has an extremum with respect to τ_R. For intermediate values of η such that $\eta \ll \eta_\infty$ yet $\eta^2 \gg 1$ the condition for maximum electron concentration, found by maximizing n_{a+} as given by Eq. (49) with respect to $\tau_R\eta$,

$$\exp(\tau_R\eta)E_1(\tau_R\eta) = 1 \quad (50)$$

or

$$\tau_R\eta = \sigma_1 n_{a1} x' = 0.431$$

Thus for x' = 10 cm we find the pressure for the greatest concentration of argon ions due to photoionization of the ground state atom is afforded when p_1 = 40 μ of mercury provided the radiation source intensity is the blackbody intensity. Because photoionization of ground state atoms is effective at low pressures, we may expect large contributions to electron density from normally present impurities that can be ionized with photons of energy less than ν_{i1}.

Experimental studies of precursor effects thus far have been concerned almost solely with measurements of electron concentration. Electrons are produced not only by photoionization of ground and excited argon atoms but, as mentioned above, also by wall photoelectric effects and impurity gases. For these reasons we believe that experimental studies require the improved discrimination that is afforded by mass and optical spectrometry if they are to promote our understanding of the precursor and other radiative effects that are associated with strong shock waves.

References

[1] Weymann, H. D., "Electron Diffusion Ahead of Shock Waves in Argon," *The Physics of Fluids*, Vol. 3, 1960, pp. 545–548.

[2] Gloerson, P., "Some Unexpected Results of Shock Heating Xenon," *The Physics of Fluids*, Vol. 3, 1960, pp. 857–870.

[3] Lederman, S. and Wilson, D. S., "Microwave Resonant Cavity Measurements of Shock Produced Electron Precursors," *AIAA Journal*, Vol. 5, No. 1, Jan. 1967, pp. 70–77.

[4] Wetzel, L., "Precursor Effects and Electron Diffusion from a Shock Front," *The Physics of Fluids*, Vol. 5, 1962, pp. 824–830.

[5] Wetzel, L., "A Feature of Precursor Ionization Profiles due to Shock Radiation," *The Physics of Fluids*, Vol. 6, 1963, pp. 750–752.

[6] Clarke, J. H. and Ferrari, C., "Gas Dynamics with Non-equilibrium Radiative and Collisional Ionization," *The Physics of Fluids*, Vol. 8, 1965, pp. 2121–2139.

[7] Holstein, T., "Imprisonment of Resonance Radiation in Gases," *Physical Review*, Vol. 83, 1947, pp. 1212–1233.

[8] Biberman, L. M. and Veklenko, B. A., "Radiative Processes Ahead of a Shock-Wave Front," *Soviet Physics, JETP*, Vol. 37, 1960, pp. 117–120.

[9] Lagar'kov, A. N. and Yakubov, I. T., "The Effect of Radiation of the State of a Gas Ahead of a Shock-Wave Front," *Optics and Spectroscopy*, Vol. 14, 1963, pp. 103–107.

[10] Tumakaev, G. K. and Lazovskaya, V. R., "Investigation of the State of Mercury Vapor in a Shock Tube by the Rozhdestvenskii Hook Method," *Soviet Physics-Technical Physics*, Vol. 9, 1965, pp. 1449–1455.

[11] Murty, S. S. R., "Effect of Line Radiation of Precursor Ionization," *Journal of Quantitative Spectroscopy and Radiative Transfer*, Vol. 8, 1968, pp. 531–554.

[12] Dobbins, R. A., "Photoexcitation and Photoionization of Argon Ahead of a Strong Shock Wave," *Radiative Gas Dynamics*, Vol. VII, AIAA Selected Reprint Series, edited by R. J. Goulard, June 1969.

[13] Breene, R. G., Jr., "Line Width," *Handbuch der Physik*, Band XXVII, Spectroskopie I, Springer-Verlag, Berlin, 1964, p. 56.

[14] Fvrsov, W. and Vlassov, A., "Zur Theorie der Verbreiterung von Spectral-Linien in Homogenem Gaz," *Physikalische Zeitschrift der Sowjetunion*, Vol. 10, 1936, pp. 378–412.

[15] Mitchell, A. C. G. and Zemansky, M. W., *Resonance Radiation and Excited Atoms*, Cambridge Press, London, 1934, pp. 93–97.

[16] Holstein, T., "Imprisonment of Resonance Radiation in Gases, II," *Physical Review*, Vol. 83, 1951, pp. 1159–1168.

[17] Alpert, D., McCoubrey, A. D., and Holstein, T., "Imprisonment of Resonance Radiation in Mercury Vapor," *Physical Review*, Vol. 76, 1949, pp. 1257–1259.

[18] Phelps, A. V., "Effect of the Imprisonment of Resonance Radiation on Excitation Experiments," *Physical Review*, Vol. 110, 1958, pp. 1362–1368.

[19] Phelps, A. V., "Diffusion, De-Excitation and Three-Body Collision Coefficients for Excited Neon Atoms," *Physical Review*, Vol. 114, 1968, pp. 1011–1024.

[20] Biberman, L. M., "On the Diffusion of Resonance Radiation," *Soviet Physics, JETP*, Vol. 17, 1947, p. 416.

[21] Biberman, L. M. and Gourevitch, I. M., "Absorption of Resonance Radiation and Formation of Metastable Atoms in Mercury Vapor," *Soviet Physics, JETP*, Vol. 20, 1950, pp. 108–116.

[22] McWhirter, R. W. P., "Spectral Intensity," *Plasma Diagnostic Techniques*, ed. by R. H. Huddlestone and S. L. Leonard, Academic Press, New York, 1965, pp. 227–237.

[23] Schlüter, D., "Die Emissionskontinua Thermischer Edelgasplasmen," *Zeitschrift fur Physik*, Vol. 210, 1968, pp. 80–91.

[24] Schlüter, D., personal communication, Oct. 23, 1967, Sternwarte Bergedorf, Hamburg.

[25] Biberman, L. M. and Norman, G. E., "Plasma Radiation due to Recombination and Bremsstrahlung Processes," *Journal of Quantitative Spectroscopy and Radiative Transfer*, Vol. 3, 1963, pp. 221–245; also Rept. GA-tr-4943, Feb. 1964, General Dynamics, San Diego.

[26] Samson, J. A. R. S., "Experimental Photoionization Cross Sections in Argon from Threshold to 280 Å," *Journal of the Optical Society of America*, Vol. 54, 1964, pp. 420–421.

[27] Mirels, H., "Test Time in Low-Pressure Shock Tubes," *The Physics of Fluids*, Vol. 6, 1963, pp. 1201–1214.

[28] Chubb, D. L., "Ionizing Shock Structure in a Monatomic Gas," *The Physics of Fluids*, Vol. 11, 1968, pp. 2363–2376.

[29] Petchek, H. and Byron, S., "Approach to Equilibrium Behind Strong Shock Waves in Argon," *Annals of Physics*, Vol. 1, 1957, pp. 270–315.

[30] Wong, H. and Bershader, D., "Thermal Equilibration Behind an Ionizing Shock," *Journal of Fluid Mechanics*, Vol. 26, 1966, pp. 459–479.

[31] Moore, C. E., "Atomic Energy Levels," Vol. I, National Bureau of Standards Circular 467, June 1949, pp. 211–215.

[32] Knox, R. S., "Excited-State Wave Functions, Excitation Energies, and Oscillator Strengths for Argon ($3p^54s$)," *Physical Review*, Vol. 110, 1958, pp. 375–381.

[33] DeLeeuw, J. H., "The Interaction of a Plane Strong Shock Wave with a Steady Magnetic Field," Rept. 49, March 1958, Institute of Aerophysics, Univ. of Toronto.

[34] Chen, C. J., "Collisional-Radiative Electron-ion Recombination Rate in Rare-Gas Plasmas," *Journal of Chemical Physics*, Vol. 50, 1969, pp. 1560–1566.

MARCH 1970 AIAA JOURNAL VOL. 8, NO. 3

Estimation of Transfer Functions Using the Fourier Transform Ratio Method

JOHN BURTON ALLEN*

Lockheed-Georgia Company, Marietta, Ga.

The advent of fast Fourier transform computational methods such as the Cooley-Tukey fast Fourier transform digital computer algorithm and coherent optical Fourier transform techniques have made computationally feasible the well-known Fourier transform ratio method of estimating transfer functions. This method estimates the transfer function by taking the ratio of the Fourier transform of finite length samples of input and response measurements. First the probability density of the error term for this method is derived in the case where the input and response are looked at as sample functions of stationary stochastic processes. Then the probability density of the error term is derived in the case where the input and response are transient in nature and hence must be considered as deterministic processes. An averaging method is then suggested to reduce the error term and a means for obtaining the probability that the error term is within certain limits is indicated.

Nomenclature

α_i = Fourier coefficient
α^2 = variance of a_i and b_i
b_i = Fourier coefficient
C = maximum value of the error term
$D(\tau)$ = lag window
$E_T(\omega)$ = error term in the estimate $\hat{H}_2(\omega)$ where the input and response signals are T sec long
$E'_T(\omega)$ = error term in the stationary case due to random noise
$E''_T(\omega)$ = error term in the stationary case due to systematic noise

Received May 2, 1968; revision received October 31, 1969. The author wishes to thank J. E. Rhodes Jr. for his many helpful discussions.

* Associate Scientist, Systems Sciences Laboratory.